INFECTION AND IMMUNITY, Sept. 1987, p. 2006–2016
0019-9567/87/092006-11$02.00/0

Vol. 55, No. 9

In Vivo Killing and Degradation of *Mycobacterium aurum* within Mouse Peritoneal Macrophages

MANUEL T. SILVA,* RUI APPELBERG, M. NAZARÉ T. SILVA, AND PAULA M. MACEDO
Centro de Citologia Experimental da Universidade do Porto, Porto, Portugal

Received 23 January 1987/Accepted 21 May 1987

We studied the in vivo killing and degradation of *Mycobacterium aurum*, a nonpathogenic, acid-fast bacillus, within macrophages after inoculation into the peritoneal cavity of CD-1 mice. The degradative process could be divided in five successive steps that were characterized on ultrastructural and cytochemical grounds and the relative contributions of which were determined by quantitative electron microscopy of samples taken at different times. The main ultrastructural alterations observed during the degradative process were ribosome disaggregation, coagulation of the cytoplasmic matrix, and change in the membrane profile from asymmetric to symmetric, with loss of the polysaccharide components from the outer layer, followed by membrane solubilization and intracellular clearing, followed by digestion of the innermost (peptidoglycan) layer of the cell wall, and at the end of the process, disorganization and collapse of the remaining layers of the cell wall. The correlation between viability and morphology indicated that the first ultrastructural signs of viability loss are cytoplasmic coagulation, change in the membrane geometry, and disappearance of ribosomes. The labeling of lysosomes of peritoneal macrophages with ferritin or by the cytochemical demonstration of inorganic trimetaphosphatase showed that fusion of lysosomes with phagosomes containing mycobacteria occurs in the phagocytes in the mouse peritoneal cavity and is already extensive as soon as 1 h after the inoculation of the bacilli.

In previous reports we described the main ultrastructural alterations exhibited by *Mycobacterium leprae* undergoing degradation by macrophages in the skin of untreated and treated lepromatous patients (24, 25) and the membrane alterations occurring in several mycobacteria damaged in vitro or in vivo (24). In previous studies, we studied the fate of cultivable mycobacteria with different degrees of pathogenicity within the phagocytes of the peritoneal cavity of several mouse strains following intraperitoneal inoculation. We found that some mycobacteria are degraded by the macrophages through a sequential process that is basically similar to that previously observed with *M. leprae* (25).

As part of a program to study the interaction of mycobacteria of different degrees of pathogenicity with experimental hosts of different degrees of susceptibility to mycobacterial infections, the work described in the present report addressed the killing and degradation of *M. aurum*, a nonpathogenic acid-fast bacillus (AFB), by macrophages in the peritoneal cavity of CD-1 mice. The choice of a nonpathogenic mycobacterium as a test microorganism for the study of mycobacterial degradation in vivo was based on the following points. (i) Our previous observations (24, 25; P. M. Macedo and M. T. Silva, XVII Annu. Meet. Soc. Port. Electron Microsc. abstr. 28, 1982) showed that the degradative processes of several mycobacteria by macrophages in vivo are ultrastructurally similar. (ii) Contrary to the situation with pathogenic mycobacteria, all *M. aurum* cells are killed and degraded by the host macrophages in the initial phases of the infection, thus making the analysis of the killing and degradation easier and more amenable to quantitation. The use of this experimental model to characterize the antimycobacterial activity of phagocytes therefore has several advantages for characterization of the antimycobacterial activity of phagocytes. These include the ability to precisely determine the chronology of the different phases of the degradative process and the ability to accurately establish the correlation between ultrastructure and viability, so that the distinction between viable and dead mycobacteria can be correctly defined on morphological grounds. Moreover, the occurrence of lysosome-phagosome fusion and its participation in the degradation of the mycobacteria can be evaluated in vivo. In contrast to most published studies on the interaction of mycobacteria and macrophages, which were carried out with in vitro models, the present work has been performed in vivo; thus the interaction of mycobacteria and macrophages was studied under the natural conditions for both the natural resistance and the immune resistance to mycobacterial infection; these conditions can be manipulated, for instance, by the use of immunosuppressed or immunoactivated hosts. The methodology used in the present work is proving useful in comparative studies, under way in our laboratory, involving other mycobacteria, including mouse pathogens, and mouse strains with different degrees of susceptibility to mycobacterial infections.

MATERIALS AND METHODS

M. aurum 14121005 from the collection of the Institut Pasteur, Paris, (kindly supplied by H. L. David) was grown in nutrient broth (Difco Laboratories) supplemented with 0.04% Tween 80 at 37°C in a rotary shaker for 24 h. The bacteria were collected from the cultures by centrifugation and washed and suspended in saline supplemented with 0.04% Tween 80. The final suspensions were lightly sonicated (50 W, 10 s; model W 185 D Branson Sonifier) and filtered through a 5-μm-pore-size membrane (6). The final suspensions were found to consist mostly of single cells, containing more than 90% viable bacteria; the actual number of viable cells in each experiment is indicated in Results. Bacterial suspensions (0.5 ml) containing a high inoculum (5×10^7 to 2×10^8 CFU), necessary for the electron-microscopic studies, were injected into the peritoneal cavity of 4- to 6-week old male CD-1 mice, which were housed under

* Corresponding author.

conventional conditions and fed commercial chow and water ad libitum. Some experiments were carried out with 4- to 6-week old female C57BL/6 mice, which were housed under the conditions indicated above. At intervals (from 1 h to 15 days) the animals were put to death by ether anesthesia, and 5 ml of Hanks balanced salt solution was injected intraperitoneally; after an abdominal massage the peritoneal fluid was collected. Ziehl-Neelsen-stained homogenates from the parathymic lymph nodes, liver, and spleen of each mouse were observed for the presence of mycobacteria. The following studies were carried out with portions of the peritoneal fluid.

Assessment of phagocytosis. Cytospin (model II Shandon Cytospin) preparations of the peritoneal exudate were stained by the Ziehl-Neelsen technique and used to determine the number of phagocytes containing ingested mycobacteria and the number of AFB per infected phagocyte. To evaluate the rate of phagocytosis of the injected mycobacteria, we determined the number of extracellular bacilli by using Ziehl-Neelsen-stained smears prepared with pellets (centrifuged at 3,000 × *g* for 10 min) from the peritoneal fluid that had been fixed (with 2.5% glutaraldehyde) immediately after collection, to prevent lysis of the phagocytes during specimen preparation.

Electron microscopy of leukocytes and mycobacteria. The cells in the peritoneal exudate were separated by centrifugation (1,000 × *g* for 2 min), and the pellet was processed for electron microscopy by fixation in 4% formaldehyde–1.25% glutaraldehyde–10 mM calcium chloride for 24 h at room temperature, then in 1% OsO_4–10 mM calcium chloride for 16 to 24 h at room temperature, and then in 1% uranyl acetate for 1 h, as described previously (20–22). Further processing for electron microscopy was carried out with ethanol dehydration and Epon embedding. Ultrathin sections were stained with lead citrate (30) for 5 min or double-stained with uranyl acetate (saturated aqueous solution) for 5 min followed by lead citrate for 3 min. The Thiéry procedure (29) was used for the ultrastructural detection of periodic acid-Schiff (PAS)-positive molecules, usually with silver vitellinate instead of silver proteinate (23, 24; M. T. Silva, P. M. Macedo, R. Salema, and I. Santos, XVII Annu. Meet. Soc. Port. Electron Microsc., abstr. 30, 1982). Tracings of membrane profiles were made on photographic negatives with a Joyce-Loebl MK III CS microdensitometer, set to an arm ratio of 50× and a slit of 0.5 nm. Whenever quantitative ultrastructural studies were to be carried out, we cut sections, taking precautions to avoid serial sectioning.

To better detect phagosome-lysosome fusion after phagocytosis of the mycobacteria by the phagocytes in the peritoneal cavity of each mouse, two procedures were used. One consisted of prelabeling the lysosomes with ferritin by the method of de Bakker (J. M. de Bakker, Ph.D. thesis, Royal University of Leiden, Leiden, The Netherlands, 1983); in brief, 1 week before mice were inoculated with mycobacteria, they were injected intraperitoneally with iron-dextran (Sigma Chemical Co.) diluted in saline so that 1 mg of iron was given to each mouse in a volume of 0.5 ml. The study of the peritoneal cell population showed that 7 days after the injection of iron-dextran the population had recovered from a brief and mild inflammatory reaction. Confirming the results of de Bakker, we found that more than 95% of the resident peritoneal macrophages (identified by their pattern of peroxidase activity [3]) had lysosomes laden with ferritin, which is a product of the conversion of the injected iron-dextran (de Bakker, thesis). The second procedure, which did not require pretreatment of the mice, consisted of the ultrastructural demonstration of inorganic trimetaphosphatase, a better lysosome marker than acid phosphatase (14), by the technique of Petty et al. (14); this technique was applied to portions of peritoneal exudates collected as described above and fixed with 1.0% glutaraldehyde in 0.1 M cacodylate buffer (pH 7.4), supplemented with 2% sucrose, for 1 h. Ferritin labeling of lysosomes has the advantage that the phagocytosed mycobacteria are better preserved, since the fixation procedure developed for analysis of bacterial ultrastructure can be used, whereas the enzymatic cytochemistry has a deleterious effect on the fine structure of the bacteria as a result of incubating and washing the samples for the cytochemical reaction before the cells are properly fixed. The ultrastructural studies were carried out with Siemens Elmiskop 1A and 102 electron microscopes.

Fate of the mycobacteria in the peritoneal cavity. We determined the total number of AFB and the viability of *M. aurum* in samples collected from the peritoneal cavity of mice as described above. Viability was determined by the plate dilution method. In brief, a portion of the exudate collected in Hanks solution was centrifuged (1,000 × *g* for 2 min) and the pelleted cells were suspended in a volume of 0.04% Tween 80 equal to the volume of the initial suspension and lightly sonicated (50 W for 15 s in a Branson Sonifier) to help the disruption of the phagocytes and disperse bacterial clumps. Preliminary experiments showed that this treatment has no deleterious effect on *M. aurum* viability. Serial dilutions of the sonic extract were plated in duplicate on nutrient agar (Difco) and incubated for 8 days at 37°C. AFB (expressed as the total number per peritoneal cavity) were counted by two procedures. (i) For the sonicated bacterial suspension used for viability studies AFB were enumerated by the technique of Shepard and McRae (16), with coated multispot microscope slides (Wellcome Research Laboratories) containing 5 μl of sonic extract in each spot and with Ziehl-Neelsen staining. This method was more satisfactory for samples with large numbers of bacilli (above 10^7 per peritoneal cavity) because the bacteria were dispersed owing to the lysis of macrophages. (ii) For the cytospin preparations of the peritoneal fluid indicated above, the number of AFB was calculated by counting the bacilli and the leukocytes; the actual number of AFB per peritoneal cavity was obtained by extrapolation from the ratio of bacilli to leukocytes, taking into account the total number of leukocytes determined as described above. This method was preferred when lower numbers of AFB (below 10^7) were present.

RESULTS

Dynamics of phagocytosis and killing of *M. aurum* in the peritoneal cavity of CD-1 mice. The enumeration of extracellular and intraphagocytic bacilli showed that phagocytosis of the inoculated bacteria is already extensive by 1 h (with more than 99% of bacilli inside phagocytes) but that it takes 4 h to go to completion. The number of AFB present in the peritoneal fluid at 4 h after inoculation was lower than the number of AFB inoculated; in two independent experiments $1.04 \times 10^7 \pm 0.32 \times 10^7$ and $1.74 \times 10^7 \pm 0.37 \times 10^7$ AFB were found after the inoculation of 8.0×10^7 and 9.7×10^7 AFB, respectively. Although such a reduction is due in part to the adherence of macrophages with ingested bacilli to the peritoneal wall, clearing of mycobacteria by lymphatic drainage occurs as deduced from the early appearance of AFB in the parathymic lymph nodes, spleen, and liver. However,

TABLE 1. Number of AFB and viable *M. aurum* cells[a]

Time (days) after inoculation	No. of bacteria/peritoneal cavity[b]		% Viable cells
	AFB	Viable cells	
4 h	$(1.44 \pm 0.49) \times 10^7$	$(1.37 \pm 0.43) \times 10^7$	95.14
1	$(1.48 \pm 0.96) \times 10^7$	$(5.25 \pm 0.83) \times 10^6$	35.47
2	$(1.36 \pm 0.85) \times 10^7$	$(4.78 \pm 0.90) \times 10^5$	3.51
4	$(1.24 \pm 0.95) \times 10^7$	$(2.73 \pm 1.30) \times 10^4$	0.22
6	$(2.10 \pm 1.06) \times 10^6$	$(2.17 \pm 1.29) \times 10^3$	0.10
8	$(1.45 \pm 1.11) \times 10^6$	$(1.25 \pm 1.05) \times 10^3$	0.09
10	$(1.22 \pm 1.13) \times 10^6$	$(7.30 \pm 5.80) \times 10^2$	0.06

[a] Number of cells in samples collected at the indicated times from the peritoneal cavity of CD-1 mice inoculated with 8.0×10^7 bacilli (96.3% viable).

[b] Values represent mean ± standard deviation of the number of bacteria per peritoneal cavity for six mice.

macrophages with ingested bacilli persisted in the peritoneal cavity for some time, and the counts of AFB in Ziehl-Neelsen-stained smears of the peritoneal exudate showed a plateau that was maintained for 4 days (Table 1). During that period the number of AFB per phagocyte was 8.70 ± 0.79, 9.01 ± 0.78, 7.67 ± 0.86, and 7.37 ± 1.40 for samples collected at 4 h, 1 day, 2 days, and 4 days, respectively, indicating that *M. aurum* is not multiplying. Consequently the progressive decline in the number of viable mycobacteria (Table 1) indicates that the bacilli are killed within the peritoneal macrophages. Such a situation gives us the opportunity to analyze the ultrastructure of the antimycobacterial activity of macrophages.

Ultrastructure of *M. aurum* organisms undergoing killing and degradation by peritoneal macrophages in CD-1 mice. Preliminary observations showed that bacteria were quite rare in samples collected after 8 days postinoculation. Ultrastructural analysis of 784 individual electron micrographs of bacillary profiles of *M. aurum* in sections from samples collected from 4 h to 8 days after inoculation showed ultrastructurally normal bacilli and bacilli under a progressive process of degradation. The following steps could be characterized.

Step 1 (Fig. 1A to C) is characterized by bacteria with normal ultrastructure (22, 24), that is, bacteria with a continuous, undeformed cell wall and cytoplasmic membrane, distinct ribosomes, and fibrillar DNA; the membranes are asymmetric after both lead (Fig. 1A and B) and Thiéry (Fig. 1C) staining.

Step 2 (Fig. 1D to F and 2A) is characterized by compact cells with a change in the membrane profile from asymmetric to symmetric, a loss of the PAS-positive components from the outer membrane layer (that is, the membrane becomes Thiéry negative) (Fig. 1F), and disorganization followed by disappearance of ribosomes and/or the presence of blocks of homogeneous material in the cytoplasm. The cell wall and the nucleoid remain unchanged.

Step 3 (Fig. 2B) is characterized by compact cells with a discontinuous, symmetric, Thiéry-negative cytoplasmic membrane, the occurrence of intracytoplasmic arrays of symmetric, Thiéry-negative membranes, a cytoplasmic matrix entirely composed of amorphous material identical to that in the blocks seen in step 2, and areas with fibrils with the characteristics of DNA. The peptidoglycan layer of the wall exhibits signs of incipient degradation such as localized thinning and small discontinuities.

Step 4 (Fig. 3A and B) is characterized by a progressive deformation of the cell wall, which appears distorted and discontinuous, indicating that peptidoglycan is being progressively digested. The cytoplasmic membrane is extensively solubilized and eventually disappears. Empty spaces appear in the cytoplasm, indicating that digestion of intracellular material is occurring. The DNA areas appear hydrated or partially digested.

Step 5 (Fig. 4A to C) is the final phase of the degradative process seen in this study, and the bacillary remnants consist of irregular, frequently broken and collapsed fragments of the wall, devoid of most or all the peptidoglycan layer. The intracytoplasmatic material is completely absent or is reduced to scant granular remnants. Although the level of cell wall remnants became too low to be detectable by electron microscopy after day 8, no images were seen that could be interpreted as corresponding to their degradation; it is possible that macrophages with such remnants leave the peritoneal cavity before the digestion, if any, of the wall material.

There is no electron-transparent zone (4) around the phagocytosed bacilli (Fig. 1A and D; Fig. 2A and B; Fig. 3A and B).

Table 2 depicts the sequence of the main ultrastructural alterations described above for the degradation process of *M. aurum* within mouse peritoneal macrophages. Figure 5 shows the results of a quantitative study of the distribution of the 784 bacilli seen in each of the morphological steps in samples collected from 4 h to 8 days. Those results show that the degradative process is not synchronous; that ultrastructural bacillary alterations occurring after the phagocytosis of bacteria begin to be observed in the 24-h sample, since the percentage of altered bacilli in the 4-h sample is similar to that of nonviable bacteria in the inoculum; and that no bacilli with normal ultrastructure are present after 2 days.

We studied in some detail the rate of appearance of the initial ultrastructural alterations, i.e., those typical of step 2, since they are likely to represent the first morphological counterpart of bacterial death (see below). We found that the only ultrastructural alteration in 13.6% of the bacilli in step 2 seen in the 24-h sample was the presence of the cytoplasmic blocks; that is these cells still have asymmetric membranes and ribosomes. The percentage of cells with cytoplasmic blocks increased progressively, reaching 100% of compact bacilli at day 4. On the other hand, all bacilli with symmetric membranes had no visible ribosomes in the samples taken at 1 day or later.

Assessment of phagosome-lysosome fusion in CD-1 and C57BL/6 mice. Lysosomes were occasionally seen in contact or undergoing fusion with the phagocytic vacuoles (Fig. 3A and 4A). The occurrence of extensive phagosome-lysosome fusion after phagocytosis of the injected mycobacteria was, however, clearly demonstrated by the use of both ferritin prelabeling of lysosomes of peritoneal resident macrophages (Fig. 6A to C) and postlabeling of lysosomes by demonstration of trimetaphosphatase activity (Fig. 6D and E), because these procedures allowed the detection of phagosome-lysosome fusion in cases in which the plane of the section did not show the actual fusion (Fig. 6C to E). The use of those lysosomal markers showed that extensive phagosome-lysosome fusion occurs in peritoneal resident macrophages soon after the inoculation of *M. aurum*. At 1 h after intraperitoneal inoculation of 2.0×10^8 *M. aurum* cells (1.9×10^8 viable cells) in CD-1 and C57BL/6 mice, the number of AFB per infected macrophage was 15.92 ± 3.30 and 15.35 ± 4.11, respectively, and the percentage of phagosomes containing mycobacteria that had fused with lysosomes (as deduced from the presence of trimetaphosphatase activity inside the phagosome) was 89.7 and 94.3%, respectively. At

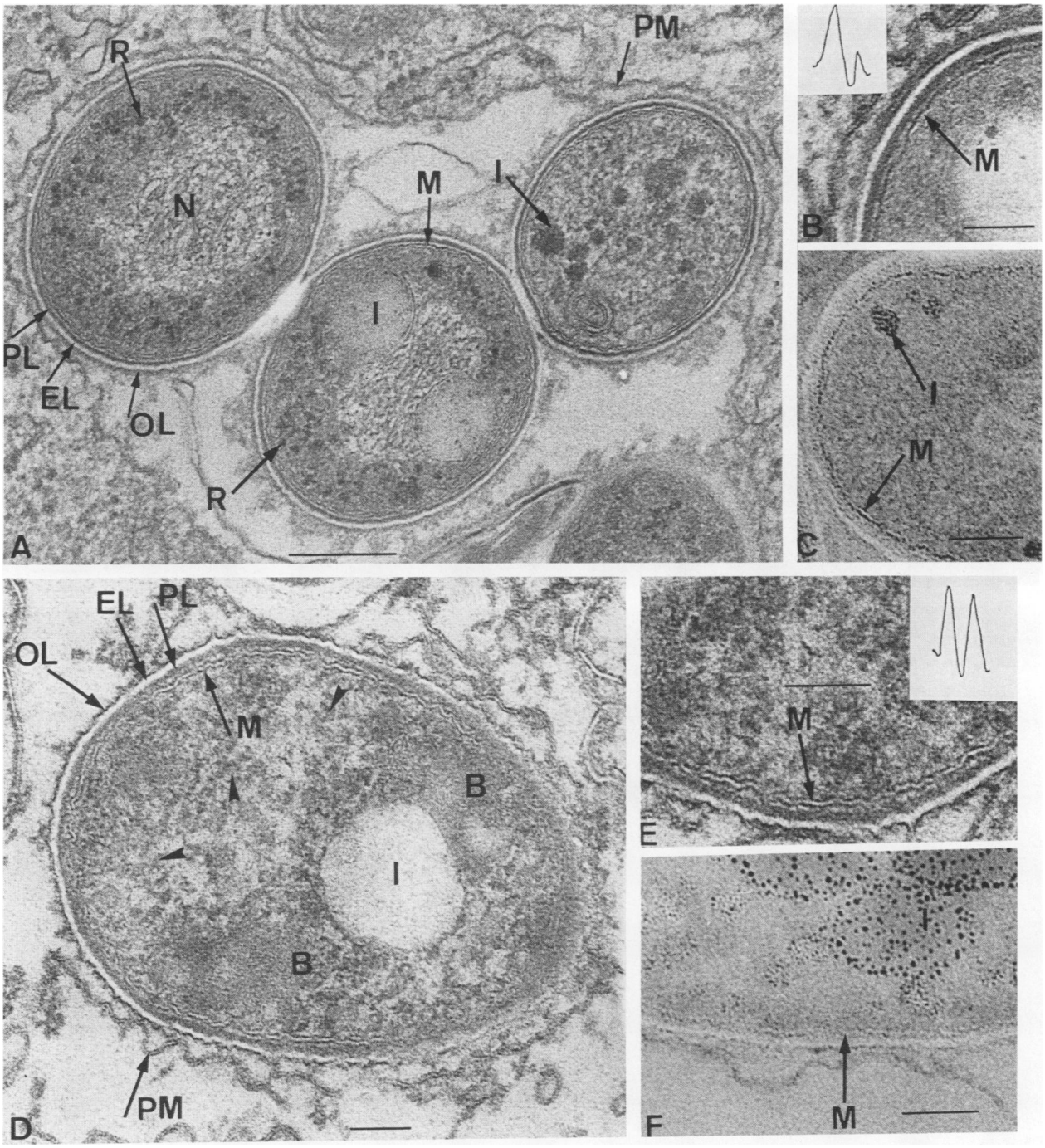

FIG. 1. (A) *M. aurum* cells within a CD-1 mouse peritoneal phagocyte in a sample collected 4 h after inoculation. The ultrastructure of the bacilli is normal (step 1). Notice the presence of distinct ribosomes (R) and the asymmetric profile of the cytoplasmic membrane (M). The cell wall, with its three layers (outer layer [OL], electron-transparent layer [EL], and peptidoglycan layer [PL]) is intact. No electron-transparent zone is present between the bacillary surface and the phagosome membrane (PM). N, Nucleoid. I, intracytoplasmic inclusions. Lead stain. Magnification, ×80,960. Bar, 0.2 μm. (B) Same sample as in panel A at a higher magnification, showing the asymmetric profile of the cytoplasmic membrane (M). The membrane profile is also represented by a densitometric tracing. Lead stain. Magnification, ×110,400. Bar, 0.1 μm. (C) Same sample as in panel A, Thiéry stained for PAS-positive molecules. The micrograph shows bacillus (step 1) with a Thiéry-positive membrane outer layer (M). There is an intracytoplasmic inclusion (I) with a positive Thiéry reaction. Magnification, ×115,920. Bar, 0.1 μm. (D) *M. aurum* cells (step 2) in a sample collected 4 days after intraperitoneal inoculation. Notice the symmetric profile of the cytoplasmic membrane (M) and the disorganized ribosomes (arrowheads). Blocks of electron-dense material are present in the cytoplasm (B). The cell wall (OL, EL, and PL) is intact. Lead stain. Magnification, ×95,680. Bar, 0.1 μm. (E) Part of the same cell as in panel D, showing at higher magnification the symmetric profile of the cytoplasmic membrane (M). The membrane profile is also represented by a densitometric tracing. Lead stain. Magnification, ×134,320. Bar, 0.1 μm. (F) Thiéry stain of a bacillus in the same sample as in panel D. Notice the Thiéry-negative profile of the cytoplasmic membrane (M) and the presence of PAS-positive inclusions. Magnification, ×115,920. Bar, 0.1 μm.

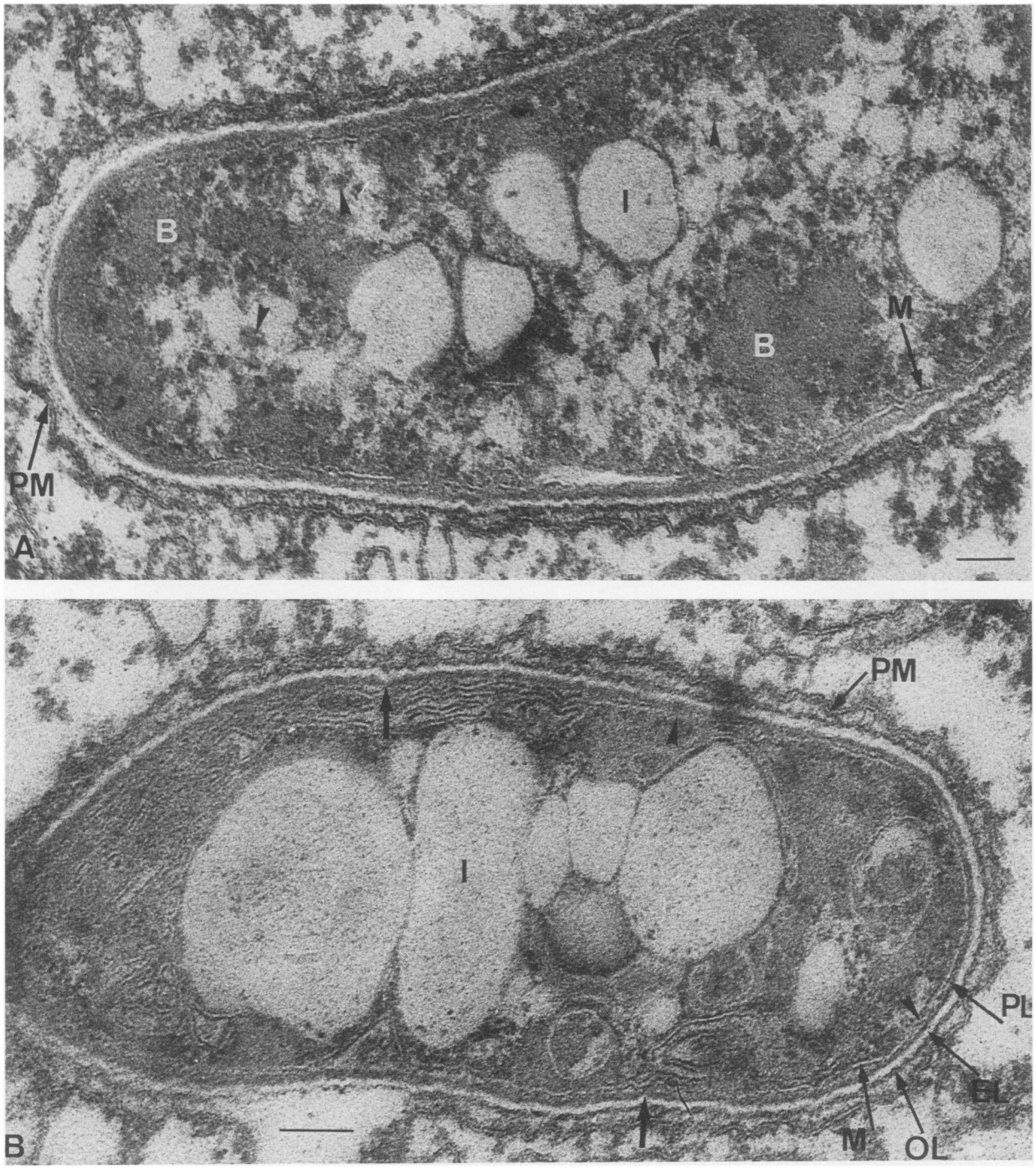

FIG. 2. (A) *M. aurum* cell at step 2 in a 4-day sample. Notice the symmetric cytoplasmic membrane (M), the absence of intact ribosomes, and the presence of dense blocks in the cytoplasm (B). The arrowheads indicate disorganized ribosomes. Uranyl-lead stain. Magnification, ×95,680. Bar, 0.1 μm. (B) *M. aurum* cell at step 3 in a 6-day sample. Notice the symmetric profile of the cytoplasmic membrane (M); this membrane is solubilized in places (arrowheads). Arrays of symmetric membranes are present in the cytoplasm. No ribosomes are visible, and the cytoplasmic matrix has the same structure as the blocks seen in step 2 cells. The peptidoglycan layer of the wall (PL) shows signs of incipient degradation (unlabeled arrows). There is no electron-transparent zone. Uranyl-lead stain. Magnification, ×114,080. Bar, 0.1 μm.

1 h after inoculation of 9.2×10^7 *M. aurum* cells (8.3×10^7 viable cells) into the peritoneal cavity of CD-1 mice, 90.2% of phagosomes containing bacilli had ferritin labeling. In samples collected later in the process, trimetaphosphatase activity and ferritin molecules were seen inside damaged mycobacteria (Fig. 6D), indicating that a severe permeabilization of the bacterial envelopes had occurred. As expected from the absence of an electron-transparent zone around the phagocytosed bacilli, the deposits revealing trimetaphosphatase activity or the ferritin molecules were seen in close contact with the mycobacterial surface (Fig. 6B to E). The same observation had been reported by others for

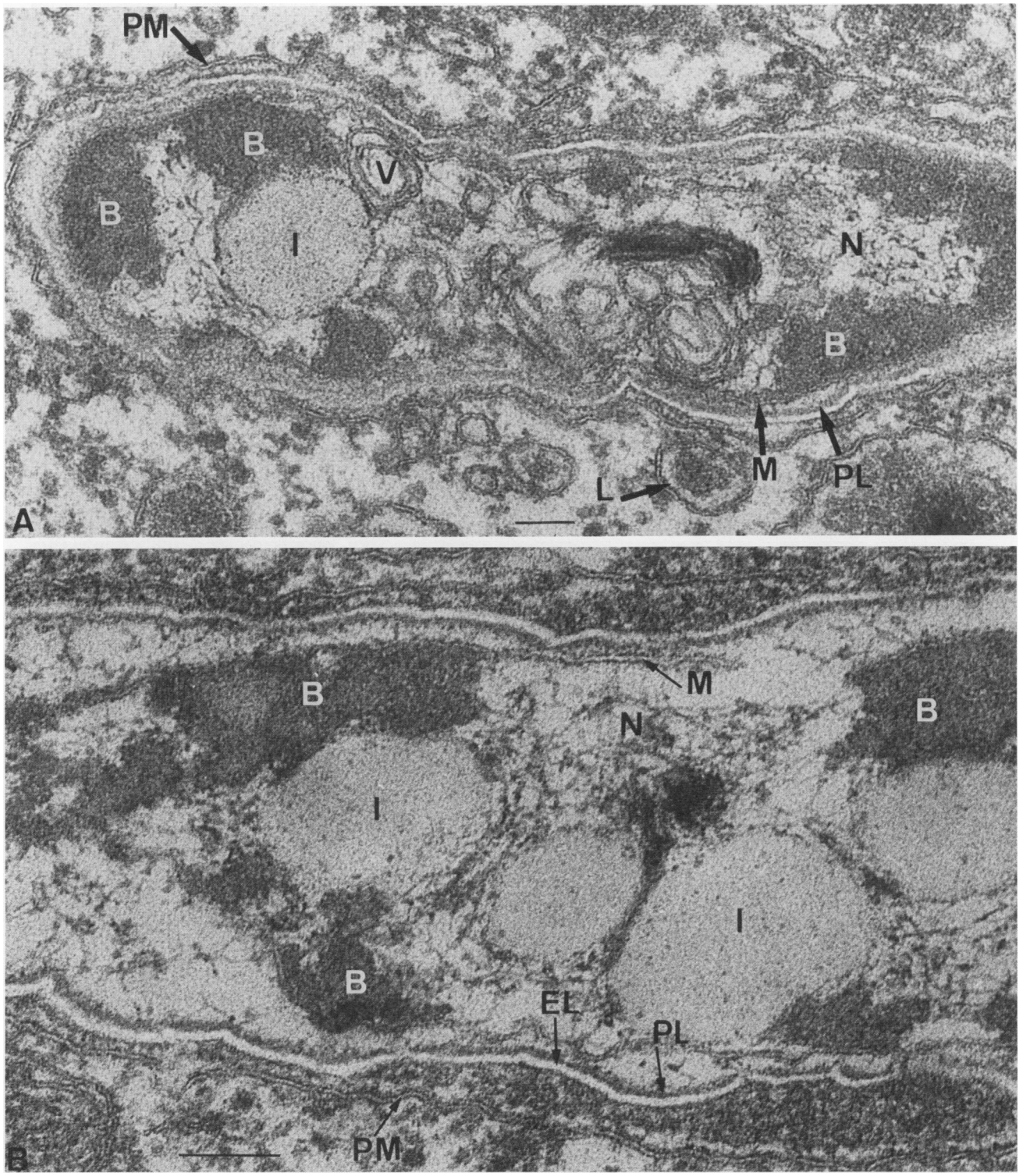

FIG. 3. (A) *M. aurum* at step 4 in a 4-day sample. Notice the deformation of the cell wall with breaks in its peptidoglycan layer (PL), the discontinuous, symmetric cytoplasmic membrane (M), and the presence of membrane vesicules in the cytoplasm (V). Blocks of homogeneous material (B) are present in the cytoplasm, which has no ribosomes and is clearing at some places. N, Areas of hydrated DNA; L, a lysosome close to the phagosome. No electron-transparent zone is present. Uranyl-lead stain. Magnification, ×104,000. Bar, 0.1 μm. (B) Part of an *M. aurum* cell at a more advanced stage 4 than in panel A. The sample was collected 6 days after the intraperitoneal inoculation. The cytoplasm is under advanced digestion, with only some blocks of dense material (B) and DNA fibrils (N) remaining. The cytoplasmic membrane (M) is extensively solubilized. The cell wall is undulated and has breaks in the peptidoglycan layer (PL). Intracytoplasmic inclusions are still present (I). Uranyl-lead stain. Magnification, ×164,000. Bar, 0.1 μm.

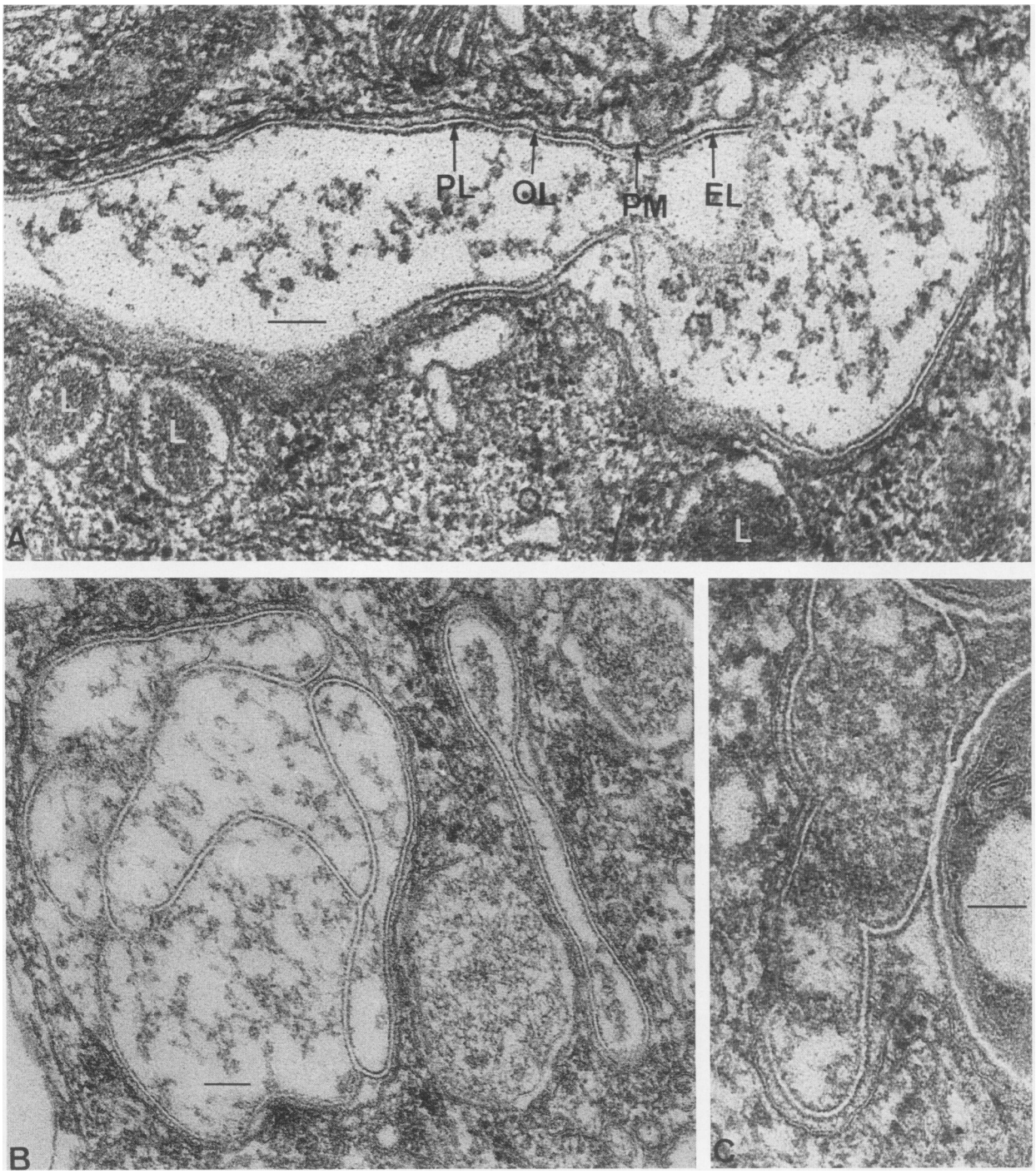

FIG. 4. (A) *M. aurum* at step 5 in a 6-day sample. Notice the bacillary ghost with a deformed cell wall consisting of the outer dense layer (OL) and the electron-transparent layer (EL) with some remnants of the peptidoglycan layer (PL) attached to the inner surface of the electron-transparent layer. The cytoplasm is reduced to scant granular material. Lysosomes (L) are in contact with the phagosome. No electron-transparent zone is present. Uranyl-lead stain. Magnification, ×95,680. Bar, 0.1 μm. (B) Deformed and collapsed cell wall remnants in *M. aurum* at step 5 in a 6-day sample. Uranyl-lead stain. Magnification, ×69,920. Bar, 0.1 μm. (C) Part of a bacillus at step 3 (right side of the picture) and a bacillary ghost at step 5. The picture clearly shows that the wall remnants typical of step 5 originate from the outer and electron-transparent layers of the wall. The sample was collected 6 days after intraperitoneal inoculation. Uranyl-lead stain. Magnification, ×92,000. Bar, 0.1 μm.

macrophages infected in vitro with *M. aurum* and with acid phosphatase as a lysosomal marker (7).

Correlation of viability and morphology in *M. aurum* cells within peritoneal macrophages in CD-1 mice. Assessment of the percentage of viable mycobacteria in the peritoneal bacillary population during the initial 10 days after inoculation of *M. aurum* (Table 1) indicates that no significant loss of viability occurs during the first 4 h, because the percent-

TABLE 2. Summary of the main ultrastructural characteristics typical of each step of the degradative process

Step	Cell wall[a]		Membranes	Cytoplasm		DNA
	EL	PL		Matrix	Ribosomes	
1	Normal	Normal	Normal	Normal	Normal	Normal
2	Normal	Normal	Asymmetric or symmetric and Thiéry negative	Normal or blocks	Normal or disorganized or absent	Normal
3	Normal	Thinner in places	Partially solubilized	Blocks	Absent	Hydrated or partially digested
4	Deformed	Deformed and partially solubilized	Extensively solubilized	Extensively digested or absent	Absent	Extensively digested or absent
5	Collapsed and deformed	Extensively solubilized or absent	Absent	Absent	Absent	Absent

[a] EL, Electron-transparent layer; PL, peptidoglycan layer.

age of viable organisms in the 4-h sample was similar to that in the inoculum. A progressive reduction in the number of viable mycobacteria occurred during the 10 days following inoculation, and no viable bacteria were found after that time. Comparison of the viability of *M. aurum* cells (Table 1) with the distribution of each of the ultrastructural steps of the degradative process of that mycobacterium inside the phagocytes during the same period (Fig. 5) shows that the percentage of viable bacilli is close to the percentage of bacilli in step 1. This suggests that only the bacilli with normal ultrastructure (step 1) are viable and that the appearance of any of the three alterations associated with step 2 is accompanied by loss of viability.

DISCUSSION

Since the *M. aurum* cells that persist in the peritoneal cavity of mice after an intraperitoneal inoculation are progressively killed and degraded by the peritoneal macrophages, we are dealing with a model that allows the in vivo quantitative and chronological study of the antimycobacterial activity of macrophages.

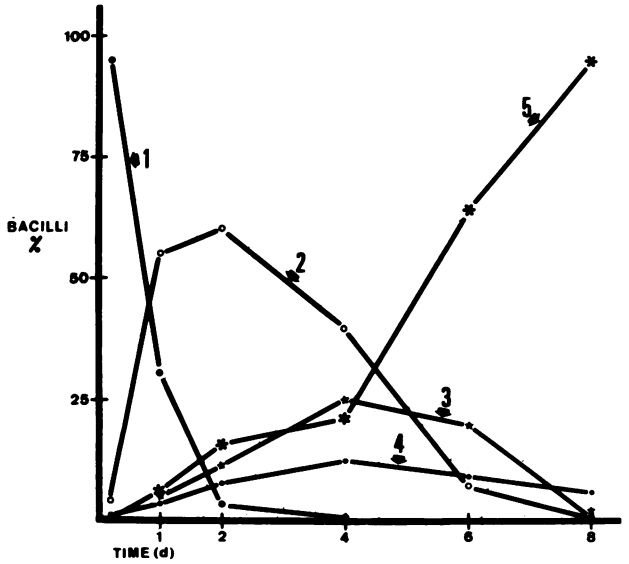

FIG. 5. Percentage of bacilli in each of the five steps (indicated by the arrows labeled 1 to 5) of the degradative process of *M. aurum* in samples taken at the indicated intervals after intraperitoneal inoculation of 8.0×10^8 bacilli (7.7×10^7 viable cells) in CD-1 mice.

The first ultrastructural alterations detected in the mycobacteria under degradation (step 2) occur in the cytoplasm and membranes and represent morphological signs of lethal bacillary damage. The asymmetric profile found in normal *M. aurum* membranes changes to a symmetric profile, and the PAS-positive components of the membrane outer layer are lost early in the degeneration process. These two membrane alterations indicate membrane damage and have been found in several situations, both in vitro and in vivo, in which gram-positive bacteria, including AFB, are damaged by lysis or by treatment with membrane-active agents (17–19, 24, 26, 27). We have previously shown that the loss of PAS-positive components from the outer layer of damaged membranes in those bacteria is associated with the change in the membrane profile from asymmetric to symmetric (19, 24). Ribosomes become invisible during the initial phase of the degradative process, and homogenous blocks appear in the cytoplasm. Ribosome disappearance has been found for several damaged gram-positive bacteria (15, 22, 27). Several mechanisms can be advanced to explain ribosome disappearance: ionic leakage associated with the loss of membrane-selective permeability as a result of membrane damage at the beginning of the degradative process (as deduced from the above reported membrane ultrastructural alterations and from the observation of deposits of trimetaphosphatase activity and of ferritin molecules inside mycobacteria under degradation), because ribosome stability depends on the intracellular ionic environment (22); activation of bacterial endogenous RNases that is known to occur in some situations of membrane damage (12, 15); and access to the bacterial cytoplasm of lysosomal RNases, facilitated by the loss of the cytoplasmic membrane permeability barrier owing to the early membrane damage. The last is a likely mechanism for that alteration in situations in which phagosome-lysosome fusion occurs, as is the case in the present study. Support for the relationship between membrane damage and ribosome disappearance implicated by the above mechanisms is obtained from our observation that bacilli without ribosomes have symmetric (altered) membranes.

The early occurrence of blocks of amorphous material in the cytoplasm of bacilli deserves some comment. This alteration, although rather discrete in morphological terms, seems to represent a lethal alteration. Such an alteration was previously found in *Bacillus cereus* cells exposed to moist heat (26) and, most interestingly, in *M. aurum* cells killed in vitro by exposure to oxygen-dependent bactericidal radicals (R. Appelberg and M. T. Silva, International Symposium on Mycobacteria of Clinical Interest, abstract 90, 1985).

From the results of our study of the correlation between

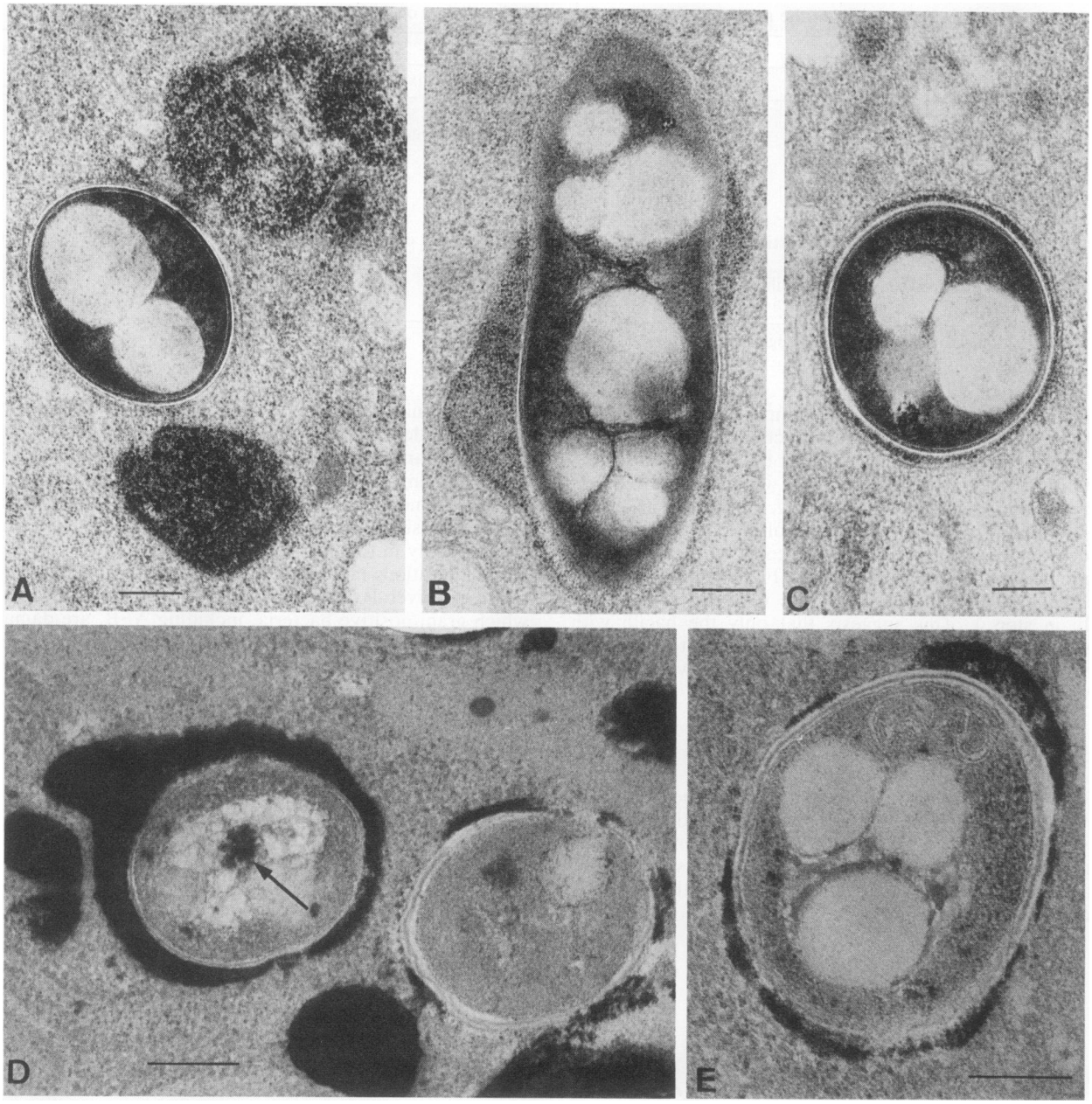

FIG. 6. (A to C) *M. aurum* cells inside peritoneal macrophages prelabeled with ferritin. The sample was collected 1 h after the intraperitoneal inoculation of 8.8×10^7 AFB (8.2×10^7 viable cells). In panel A, two heavily labeled lysosomes are close to the phagosome containing a bacillus, but there is no ferritin in the phagosome, indicating that phagosome-lysosome fusion had not occurred. In panel B, the plane of the section clearly shows fusion of a lysosome with a phagosome containing one bacillus. In panel C, there is a phagosome containing one bacillus and ferritin in the space between the phagosome membrane and the surface of the mycobacterium, indicating that phagosome-lysosome fusion had occurred although no such fusion is visible in the plane of the section. Sections were lightly stained with lead to increase the relative contrast of ferritin. Magnification, ×46,920. Bar, 0.2 μm. (D and E) Trimetaphosphatase activity in peritoneal macrophages with ingested *M. aurum* cells. The sample was collected 24 h after intraperitoneal inoculation of 9.5×10^7 AFB (8.7×10^7 viable cells). The presence of the lysosomal enzymatic activity around the mycobacteria indicates that they are inside phagolysosomes. The unlabeled arrow indicates trimetaphosphatase activity inside a bacillus. Sections were lightly stained with lead. Magnification, ×67,712 (panel D), ×78,200 (panel E). Bar, 0.2 μm.

ultrastructure and viability, we conclude that mycobacterial death inside the macrophages occurs before the disaggregation of the bacilli; that is, bacterial death precedes bacteriolysis, so that dead bacilli may have a compact structure (cells at steps 2 and 3). As stressed in previous reports from this group on the ultrastructure of mycobacterial cells (19, 20, 22), the present work shows that correct methodology is essential for a significant micromorphological analysis of normal and damaged mycobacteria. For example, some of the alterations described as typical of steps 2 and 3, namely absence of ribosomes and change in membrane geometry, are found in normal bacilli when fixation is inadequate (20,

22). It has often been assumed in the past that compact mycobacterial profiles correspond to normal (sometimes referred to as viable) bacilli and that only the bacteria undergoing lysis are scored as damaged (and nonviable). Our results show that compact bacilli can have ultrastructural alterations that are incompatible with viability, as is the case with mycobacteria in steps 2 and 3.

The alterations observed after step 3 can be interpreted in terms of progressive digestion of dead bacterial cells. The hydrolytic enzymes of the macrophage lysosomes are likely to be responsible for this digestion. Extensive and early fusion of lysosomes with phagosomes containing mycobacteria was observed in the present study. On the other hand, it has been found that in vitro autolysis of mycobacteria with significant cell clearing takes much longer than the lysis we observed in the present in vivo study: mycobacteria killed by exposure to rifampin or sodium azide, or dying during the decline phase of broth cultures, remain compact for weeks (24). Moreover, in vitro experiments have shown that hydrolysis of the cell wall peptidoglycan by mycobacterial endogenous autolysins is not accompanied by significant cell clearing (10) and is almost completely inhibited at low pH (10), which is known to prevail inside macrophage phagolysosomes (8, 9). In other words, the degradation of mycobacterial cells inside macrophage phagocytic vacuoles, whenever it occurs, seems to be due to heterolysis (28) rather than to autolysis.

In *M. aurum* the peptidoglycan layer is the last structure to be completely solubilized during degradation by macrophages, leaving the electron-transparent layer and the outermost electron-dense layer of the wall as remnants of the mycobacterial cell. This observation confirms previous results regarding the resistance to degradation of the mycobacterial wall components (25).

It is known that bacterial killing within phagosomes can occur in the absence of lysosome-phagosome fusion, since the phagosome membrane has the capacity to generate antibacterial oxygen-dependent mechanisms (2, 5, 11). The fusion of lysosomes with phagosomes, however, amplifies the antibacterial capacity of the phagocyte by releasing into the phagosome several lysosomal constituents that increase the killing activity of the phagosome (1). On the other hand, the formation of phagolysosomes is necessary for bacterial degradation, because the hydrolytic enzymes involved in bacterial degradation are stored in the lysosomes. Our observation that lysosomes fuse with phagosomes containing *M. aurum* rather early and extensively indicates that the full armamentarium of the mouse peritoneal phagocytes is operating from the beginning in the control of the infection. Moreover, *M. aurum* has no electron-transparent zone, a structure that has been considered to be a protective barrier, preventing the access of the antibacterial agents of the phagosome and phagolysosome to the phagocytosed mycobacteria (4). All these observations explain the rapid killing and degradation rates of *M. aurum* within the peritoneal phagocytes of CD-1 mice. This is in contrast to the situation described for pathogenic mycobacteria, which have several efficient evasion mechanisms that allow them to survive or multiply inside the host macrophages (1).

In a recent publication, Frehel et al. (7) reported on the extent of phagosome-lysosome fusion in bone marrow-derived macrophages from C57BL/6 mice infected in vitro with the same strain of *M. aurum* used in the present study. The results of their studies showed that at the early stages of the infection only 60 to 70% of the phagosomes containing mycobacteria had fused with lysosomes. This contrasts with the value of 94.3% we found in the present study for peritoneal macrophages in the same mouse strain. Several possibilities can be put forward to explain the above differences, including the different origin of the macrophages used in the two studies (peritoneal cavity versus bone marrow), the use of in vivo versus in vitro conditions, and the use of inorganic trimetaphosphatase versus acid phosphatase for labeling the lysosomes.

In essence, the ultrastructural alterations now described for *M. aurum* undergoing degradation within mouse peritoneal macrophages follow a sequence similar to that previously reported for *M. leprae* degenerating within skin macrophages of untreated lepromatous patients (24, 25), another situation in which dead mycobacteria are degraded within phagolysosomes (13).

ACKNOWLEDGMENTS

We are grateful to M. Irene Barros, Emanuel Monteiro, and Jorge Pedrosa for excellent technical assistance.

This work was supported by grants from the Damien Foundation (Brussels), Junta Nacional de Investigaçao Científica e Tecnológia (contract 435.12.110), Instituto Nacional de Investigaçao Científica (contract 83/CEN/12), and Fundação Calouste Gulbenkian (grant to P.M.M.). The Siemens Elmiskop 102 used in the present work was a gift from Volskwagenwerke Stiftung, Hanover, Federal Republic of Germany.

LITERATURE CITED

1. **Andrew, P. W., P. S. Jackett, and D. B. Lowrie.** 1985. Killing and degradation of microrganisms by macrophages, p. 311–335. *In* R. T. Dean and W. Jessup (ed.), Mononuclear phagocytes: physiology and pathology. Elsevier Biomedical Press, Amsterdam.
2. **Babior, B. M.** 1978. Oxygen-dependent microbial killing by phagocytes. N. Engl. J. Med. **298**:659–668.
3. **Daems, W. T., D. Roos, T. J. C. van Berkel, and H. J. van der Rhee.** 1979. The subcellular distribution and biochemical properties of peroxidase in monocytes and macrophages, p. 463–514. *In* J. T. Dingle, I. H. Shaw, and P. J. Jacques (ed.), Lysosomes in applied biology and therapeutics, vol. 6. Elsevier/North-Holland Publishing Co., Amsterdam.
4. **Draper, P., and R. J. W. Rees.** 1970. Electron-transparent zone of mycobacteria may be a defense mechanism. Nature (London) **228**:860–861.
5. **Elsbach, P., and J. Weiss.** 1985. Oxygen-dependent and oxygen-independent mechanisms of microbicidal activity of neutrophils. Immunol. Lett. **11**:159–163.
6. **Forget, A., E. Skamene, P. Gros, A.-N. Miailhe, and R. Turcotte.** 1981. Differences in response among inbred mouse strains to infection with small doses of *Mycobacterium bovis* BCG. Infect. Immun. **32**:42–47.
7. **Frehel, C., C. de Chantelier, T. Lang, and N. Rastogi.** 1986. Evidence for inhibition of fusion of lysosomal and prelysosomal compartment with phagosomes in macrophages infected with pathogenic *Mycobacterium avium*. Infect. Immun. **52**:252–262.
8. **Geisow, M. J., P. D'Arcy Hart, and R. Young.** 1981. Temporal changes in lysosome and phagosome pH during phagolysosome formation in macrophages: studies by fluorescence microscopy. J. Cell Biol. **89**:645–652.
9. **Jackes, Y. V., and D. F. Gaiton.** 1978. Changes in pH within phagocytic vacuoles of human neutrophils of monocytes. Lab. Invest. **39**:179–185.
10. **Kilburn, J. O., and G. K. Best.** 1977. Characterization of autolysins from *Mycobacterium smegmatis*. J. Bacteriol. **129**: 750–755.
11. **Klebanoff, S. J.** 1980. Oxygen metabolism and the toxic properties of phagocytes. Ann. Intern. Med. **93**:480–489.
12. **Lambert, P. A., and A. R. W. Smith.** 1976. Antimicrobial action of dodecyldiethanolamine: activation of ribonuclease 1 in *Esch-*

erichia coli. Microbios **17**:35–49.
13. **Mor, N.** 1983. Intracellular location of *Mycobacterium leprae* in macrophages of normal and immunodeficient mice and effect of rifampin. Infect. Immun. **42**:802–811.
14. **Petty, H. R., W. Hermann, and H. M. McConnell.** 1985. Cytochemical study of macrophage lysosomal inorganic trimetaphosphatase and acid phosphatase. J. Ultrastruct. Res. **90**:80–88.
15. **Santos-Mota, J. M., M. T. Silva, and F. Carvalho-Guerra.** 1971. Ultrastructural and chemical alterations induced by dicumarol in *Streptococcus faecalis*. Biochim. Biophys. Acta **249**:114–121.
16. **Shepard, C. C., and D. H. McRae.** 1968. A method for counting acid-fast bacteria. Int. J. Lepr. **36**:78–82.
17. **Silva, M. T.** 1967. Electron microscopic aspects of membrane alterations during bacterial cell lysis. Exp. Cell Res. **46**:245–251.
18. **Silva, M. T.** 1975. The ultrastructure of the membrane of Gram-positive bacteria as influenced by fixatives and membrane-damaging treatments, p. 255–289. *In* R. M. Burton and L. Packer (ed.), Biomembranes: lipids, proteins and receptors. BI-Science Publications, Webster Groves, Mo.
19. **Silva, M. T.** 1984. The use of transmission electron microscopy of ultrathin sections for the characterization of normal and damaged bacterial membranes, p. 1–36. *In* F. C. Guerra and R. M. Burton (ed.), Biomembranes: dynamics and biology. Plenum Publishing Corp., New York.
20. **Silva, M. T., and P. M. Macedo.** 1982. Ultrastructure of *Mycobacterium leprae* and other acid-fast bacteria as influenced by fixation conditions. Ann. Microbiol. (Paris) **133B**:59–73.
21. **Silva, M. T., and P. M. Macedo.** 1983. Electron microscopic study of *Mycobacterium leprae* membrane. Int. J. Lepr. **51**:219–224.
22. **Silva, M. T., and P. M. Macedo.** 1983. The interpretation of the ultrastructure of *Mycobacterium* cells in transmission electron microscopy of ultrathin sections. Int. J. Lepr. **51**:225–234.
23. **Silva, M. T., and P. M. Macedo.** 1983. A comparative ultrastructural study of the membranes of *Mycobacterium leprae* and of cultivable *Mycobacteria*. Biol. Cell. **47**:383–386.
24. **Silva, M. T., and P. M. Macedo.** 1984. Ultrastructural characterization of normal and damaged membranes of *Mycobacterium leprae* and of cultivable mycobacteria. J. Gen. Microbiol. **130**:369–380.
25. **Silva, M. T., P. M. Macedo, M. H. Costa, H. Gonçalves, J. Torgal, and H. L David.** 1982. Ultrastructural alterations of *Mycobacterium leprae* in skin biopsies of untreated and treated lepromatous patients. Ann. Microbiol. (Paris) **133B**:75–92.
26. **Silva, M. T., and J. C. F. Sousa.** 1972. Ultrastructural alterations induced by moist heat in *Bacillus cereus*. Appl. Microbiol. **24**:463–476.
27. **Silva, M. T., J. C. F. Sousa, J. J. Polónia, and P. M. Macedo.** 1979. Effects of local anesthetics on bacterial cells. J. Bacteriol. **137**:461–468.
28. **Stolp, H., and M. P. Starr.** 1965. Bacteriolysis. Annu. Rev. Microbiol. **19**:79–104.
29. **Thiéry, J. P.** 1967. Mise en évidence des polysaccharides sur coupes fines en microscopie électronique. J. Microsc. (Paris) **6**:987–1018.
30. **Venable, J. H., and R. Coggeshal.** 1965. A simplified lead citrate stain for use in electron microscopy. J. Cell Biol. **25**:407–408.